HHS Public Access

Author manuscript

Neurobiol Aging. Author manuscript; available in PMC 2019 November 01.

Published in final edited form as:

Neurobiol Aging. 2018 November ; 71: 41–50. doi:10.1016/j.neurobiolaging.2018.06.013.

Heterogeneity of structural and functional imaging patterns of advanced brain aging revealed via machine learning methods

Harini Eavani[#a], **Mohamad Habes**[#a,*], **Theodore D. Satterthwaite**[b], **Yang An**[c], **Meng-Kang Hsieh**[a], **Nicolas Honnorat**[a], **Guray Erus**[a], **Jimit Doshi**[a], **Luigi Ferrucci**[c], **Lori L. Beason-Held**[c], **Susan M. Resnick**[#c], and **Christos Davatzikos**[#c]

[a]Center for Biomedical Image Computing and Analytics, University of Pennsylvania, Philadelphia, PA, USA

[b]Department of Psychiatry, Brain Behavior Laboratory, University of Pennsylvania, Philadelphia, PA, USA

[c]National Institute on Aging, Baltimore, MD, USA

[#] These authors contributed equally to this work.

Abstract

Disentangling the heterogeneity of brain aging in cognitively normal older adults is challenging, as multiple co-occurring pathologic processes result in diverse functional and structural changes. Capitalizing on machine learning methods applied to magnetic resonance imaging data from 400 participants aged 50 to 96 years in the Baltimore Longitudinal Study of Aging, we constructed normative crosssectional brain aging trajectories of structural and functional changes. Deviations from typical trajectories identified individuals with resilient brain aging and multiple subtypes of advanced brain aging. We identified 5 distinct phenotypes of advanced brain aging. One group included individuals with relatively extensive structural and functional loss and high white matter hyperintensity burden. Another subgroup showed focal hippocampal atrophy and lower posterior-cingulate functional coherence, low white matter hyperintensity burden, and higher medial-temporal connectivity, potentially reflecting high brain tissue reserve counterbalancing brain loss that is consistent with early stages of Alzheimer's disease. Other subgroups displayed distinct patterns. These results indicate that brain changes should not be measured seeking a single signature of brain aging but rather via methods capturing heterogeneity and subtypes of brain aging. Our findings inform future studies aiming to better understand the neurobiological underpinnings of brain aging imaging patterns.

[*]Corresponding author at: University of Pennsylvania, Section of Biomedical Image Computing and Analysis (SBIA), Richards Building, 7th Floor, 3700 Hamilton Walk, Philadelphia, PA 19104, USA. Tel.: +1 734 478 8540; fax: +1 215 573 1811, habesm@uphs.upenn.edu (M. Habes).

Disclosure statement

None of the authors report any financial interests or potential conflicts of interest relevant to this article.

Appendix A. Supplementary data

Supplementary data associated with this article can be found, in the online version, at https://doi.org/10.1016/j.neurobiolaging.2018.06.013.

Keywords

Heterogeneity brain aging; Functional connectivity; Structural MRI; Functional connectivity; Resting-state fMRI

1. Introduction

Aging leads to highly complex changes in brain structure and function. Previous studies have shown that structural brain aging is associated with pronounced and well-characterized patterns of gray matter (GM) loss, particularly in frontal and parietal lobes (Rachael et al., 2003; Resnick et al., 2003), in addition to vascular-related brain changes in the white matter (Habes et al., 2016a; Prins and Scheltens, 2015). Functional changes in the aging brain were also reported, with the most consistent effects observed as alterations of connectivity in the default mode (DM) network (Dennis and Thompson, 2014). Importantly, age is widely accepted as a major risk factor for neurodegenerative diseases, including Alzheimer's disease (AD). Age-related neuropathologies may cause differential cognitive decline trajectories (Boyle et al., 2017), suggesting involvement of heterogeneous processes that cause structural changes and alterations in functional connectivity, seen as intermediate phenotypes between pathology and symptoms (Pievani et al., 2011).

In many studies, the target is to derive a single unifying signature/imaging pattern of normative brain aging, for example, using univariate approaches (Raz et al., 2005; Resnick et al., 2003) or multivariate predictive models using machine learning to estimate the "brain age" of healthy aging individuals from magnetic resonance (MR) images with 1 modality (Franke et al., 2010; Gaser et al., 2013; Habes et al., 2016b) or multiple modalities (Cherubini et al., 2016; Cole and Franke, 2017; Liem et al., 2017). Previous approaches enabled capturing of individuals with excessive brain changes related to aging and motivated further analysis of potential hidden heterogeneity. Approaches that explicitly model the heterogeneity of brain aging may help in better elucidating underlying pathophysiological processes in aging. Identification of patient subgroups beyond the existing clinical categorizations might be particularly important in precision medicine for specific therapeutic interventions (Whitwell et al., 2007).

In this article, we studied the heterogeneity of advanced brain aging (ABA) by applying an advanced multivariate pattern analysis method on structural and functional image data from 400 cognitively normal participants acquired as part of the Baltimore Longitudinal Study of Aging (BLSA). We first calculated brain aging indices from structural magnetic resonance imaging (sMRI) and resting-state functional magnetic resonance imaging (rsfMRI) data. It is anticipated that advanced agers will "fall off" the typical brain aging curves in multiple ways, depending on co-morbidities such as vascular disease, on intrinsic brain structural changes seen in AD, and on individual resilience to neurodegeneration. Therefore, we hypothesize that individuals who show evidence of ABA, that is, based on being "older" in terms of brain magnetic resonance imaging (MRI) scans, are in fact composed of a heterogeneous mix of multiple groups, with each group reflected by a different combination of imaging patterns.

To characterize this heterogeneity, we used a recently developed Mixture of Experts (MOEs) method (Eavani et al., 2016), which combines unsupervised modeling of mixtures of distributions with supervised learning of classifiers. Notably, we used this method to evaluate both structural and functional heterogeneity simultaneously. Unlike commonly used mass-univariate group analyses or multivariate classifiers like Support Vector Machines, which all tend to identify only a common denominator of brain variation between 2 groups, MOE combines clustering and classification to uncover multiple patterns distinguishing between groups of individuals.

2. Methods and materials

2.1. Participants

We included in our analyses 400 participants from the BLSA study with both sMRI and rsfMRI modalities with age range 50—96 years (mean ± standard deviation; 72.5 ± 9.4 years). Details of the sample and the exclusion criteria are explained in the Supplementary Materials.

2.2. Cognitive tests

BLSA participants received a battery of cognitive tests at every visit (Driscoll et al., 2006). Tests included the following: (1) California Verbal Learning Task to assess verbal learning and memory; (2) Benton Visual Retention Test quantifies visual perception, visual memory, and visuoconstructive abilities; (3) card rotations test measures the ability to mentally manipulate figures; (4) Letter Fluency measures phonemic fluency; (5) Category Fluency measures semantic fluency; (6) Trail Making Test Part A is an indicator of visual attention and processing speed; (7) Trail Making Test Part B additionally evaluated executive function; (8) Digit Symbol Test was a complex test of perceptual-motor integration and speed, and executive function.

Cognitive data were available from multiple assessments for each participant over up to a 19-year period before, and concurrent with, the time of the MRI scan. However, participants have varying numbers of visits and cognitive assessments. Therefore, every participant's cognitive performance on each of the 8 measures is summarized using 2 measurements—concurrent (with the imaging session) performance and longitudinal rate of change. Further details on cognitive testing and measures in BLSA can be found in the Supplementary Materials.

Cognitive tests were not used for identification of aging-related heterogeneity in the data set but to investigate the cognitive correlates of our image-based analysis with independent data sources.

2.3. MRI data

MRI scans were acquired at the National Institute on Aging clinical research facility on a Philips Achieva 3T MRI scanner. sMRI images were acquired using a standard magnetization-prepared rapid gradient echo acquisition with voxel size of 1 mm, and repetition time (TR)/echo time (TE) = 6.5/3.1 ms and rsfMRI with an in-plane resolution of

3 × 3 mm, slice thickness of 4 mm, TR/TE = 2000/30s, and total scan duration of 6 minutes. A fluid- attenuated inversion recovery (FLAIR) scan with voxel size of 0.83 mm, slice thickness of 3 mm, and TR/TE = 11,000/68 ms was used to assess white matter hyperintensity (WMH) burden.

2.4. rsfMRI preprocessing and parcellation

Functional time-series were slice time—corrected, realigned, and band-pass filtered to retain frequencies between 0.01 and 0.08 Hz. We applied a validated confound regression procedure that has been optimized to reduce the influence of motion using a 36 parameters regression model (Ciric et al., 2017; Satterthwaite et al., 2013). Participants who had a Mean Relative Displacement value of greater than 0.2 mm were excluded from subsequent analysis. The improved confound regression pipeline also incorporated temporal censoring (scrubbing) to remove highmotion volumes based on their frame-wise displacement and the derivative of the temporal variance of time courses. The global signal was regressed out of the voxel-wise data, as it is known to be a good surrogate measure for the effect of motion and other physiological effects on Blood-oxygen-level dependent imaging signal. Please see further details of the functional magnetic resonance imaging pre-processing pipeline in the Supplementary Materials.

We used Geodesic Graph-based Segmentation with Shape Priors, a data-driven functional parcellation method based on local functional connectivity of the voxels (Honnorat et al., 2015) to define 583 regions of interest (ROIs). A functional connectivity matrix, which encodes the correlations of average time-series between any pair of ROIs, was calculated for each study participant. Geodesic Graph-based Segmentation is open source and available online at http://www.med.upenn.edu/sbia/grasp.html.

2.5. Functional connectivity attributes

We used sparsity-based dimensionality reduction using a previously published and validated approach to reduce the high dimensionality of the functional connectivity data (Eavani et al., 2015) The data-driven method inputs the connectivity matrices from a group of individuals and automatically calculates a low-rank decomposition into a set of distinct functional subnetworks or “Sparse Connectivity Patterns” (SCPs). SCP coefficients reflect the connectivity within respective SCPs in each individual subject, that is, the degree to which a respective connectivity pattern captured by an SCP is present in an individual. SCP coefficients were calculated using the SCPLearn toolbox, which is available online at https://www.cbica.upenn.edu/sbia/software/SCPLearn/.

2.6. Regional functional coherence

Average functional coherence values were computed using the regional homogeneity index (ReHo) (Zang et al., 2004). ReHo measures the similarity of a voxel’s time series to those of its nearest neighbors. As such, it is a complementary source of information, as SCP coefficients measure long-range connectivity and coherence values measure local connectivity.

2.7. Regional volumetric attributes

Brain structure was quantified by calculating regional volumes of the aforementioned 583 ROIs for each study participant.

2.8. WMH burden

WMH were segmented from structural MR images using a multimodal supervised classification algorithm (Lao et al., 2008). The segmentation method involved co-registration of T1 and FLAIR scans, histogram normalization to a template image, feature extraction, voxelwise label assignment based on a pretrained model, and false-positive elimination. The segmentation algorithm was fully automated, and it did not require manual editing or corrections. From the 400 individuals included in our analyses, WMH load could not be calculated for 8 individuals due to lack of FLAIR images.

Details of image processing for extraction of structural and functional MR imaging features are presented in the Supplementary Information.

2.9. Age-related differences in structure and function

Correlations between each of the structural and functional attributes and age were examined via Pearson correlation coefficients and corrected for multiple comparisons using False Discovery Rate correction (Benjamini and Hochberg, 1995).

2.10. Brain aging indices of structure and function

We used a multivariate pattern regression method based on Support Vector Regression to calculate individualized brain aging scores for each study participant, which we called the Spatial Patterns of Brain Alteration for capturing Brain Aging similar to Habes et al., 2016b. We calculated the Spatial Patterns of Brain Alteration for capturing Brain Aging indices separately for structural and functional attributes, that is, using regional volumetric measures for structure, and SCP coefficients and functional coherence measures for function, with the assumption that this would allow us to identify a broader range and distinct dimensions of deviations from typical aging. The proposed approach is also supported by Sheline and Raichle, 2013, which showed that age-related structural and functional brain changes may not occur in synchrony. All models were run with cross-validation.

2.11. Resilient versus advanced agers

In the remainder of the article, the study participants who presented functional and structural brain age indices smaller than their actual age will be referred as “resilient agers.” These individuals displayed super-normal structure and function for their respective ages. We considered all other individuals to be advanced agers, as at least one of their aging patterns was lagging relative to the typical curves.

2.12. Identification of ABA subgroups using MOE

We applied the MOE method using all imaging attributes (structural and functional combined) as the input feature set for each study participant, after correcting them for age.

Resilient aging group was used as the reference group, and the ABA group as the target group, within which subgroups are detected.

The method is applied using 10-fold cross-validation. The optimal number of subgroups was determined based on reproducibility of subgroups, measured using the Adjusted Rand Index (Brouwer, 2009), and separation between subgroups, measured using the Bezdek Participation Coefficient (Bezdek, 1981; Dave, 1996). Fuzzy group membership assignments for the final model were converted to binary hard assignments. Details on the MOE approach have been presented in the Supplementary Information.

2.13. Between-subgroup differences in structure, function, WMH burden, and cognition

Cortical patterns of atrophy associated with each aging subgroup were detected through voxelwise comparisons of group differences in GM density maps against the resilient aging group. Differences in functional connectivity and coherence were examined similarly through univariate comparisons with the resilient aging group. Total WMH burden for ABA subgroups and resilient agers were compared using 2-group t-tests. The concurrent cognitive performance and longitudinal rate of change in cognition (using data beginning 10 years before the imaging visits) were compared to resilient agers using linear mixed models. F-tests were used to test the null hypothesis that all the groups were equal, followed by post hoc t-tests to compare each ABA subgroup to the resilient group.

3. Results

3.1. Age-related differences in structure and function

Age was associated with widespread GM atrophy globally. We also found reduced ReHo in posterior cingulate, dorsolateral cortex, visual cortex, and insula (Fig. 1). Four SCPs showed association with age ($p < 0.05$, Bonferroni corrected, Fig. 2).

3.2. Determination of the ABA group

Spatial Patterns of Brain Alteration models could predict the actual age of study participants with a mean average error = 4.41 and Pearson's correlation coefficient R = 0.80 for the structural model, and mean average error = 5.54 and R = 0.68 for the functional model (Fig. 3). We quantified the deviation of each aging index from typical curves by calculating their residuals against the linear fit to actual age. Structural and functional brain aging deviations form typical trends were significantly correlated ($p < 10—13$, R = 0.35). Resilient and ABA groups are determined based on the residuals of the brain aging indices (Fig. 4).

3.3. Group differences between resilient aging versus ABA groups

To describe regional effects of advanced aging beyond the average aging effect, we performed standard voxelwise 2-group comparisons, adjusting for age in all MRI measurements. As would be expected, ABA participants differed in a number of regions from the resilient group. Relative to resilient individuals, advanced agers showed significant GM atrophy in the bilateral thalamus, hippocampus, amygdala, fronto-orbital cortex, precuneus, and insula. Bilateral caudate, thalamus, and anterior insula also showed significantly lower coherence in advanced individuals relative to resilient individuals.

Among features summarizing functional connectivity, only 1 SCP showed a significant difference between the 2 groups (Fig. 5).

3.4. ABA subgroups

We found 5 distinct subgroups of ABA, with mutually exclusive sets of advanced agers associated with each subgroup. The 5 groups are reproducible (adjusted rand: 0.49 ± 0.20), well separated (Bezdek Partition Coefficient: 0.76 ± 0.21), and are reasonably classified from the resilient group (accuracy: 74.0 ± 5%). All results were obtained using 10-fold cross-validation, to ensure that models derived herein are tested on separate individuals from the ones used to derive them.

There were no significant age or sex differences among the 5 groups of advanced agers (for each group's age, gender, and motion distribution, see Table 1).

We found significant and distinctive patterns of structural and functional differences ($p < 0.05$, corrected for multiple comparisons) between each ABA subgroup and the resilient agers (Fig. 6). Note that these differences are beyond the more general age- related differences observed across the entire sample (shown in Figures 1, 2).

Group 1 consisted of 71 advanced agers who showed significantly more GM atrophy in the medial temporal lobe (MTL), including the hippocampus, parahippocampal gyrus, and amygdala bilaterally. The thalamus, caudate, superior temporal gyrus, inferior frontal GM, superior precentral gyrus, and cerebellum also showed significant atrophy. Coherence was significantly lower in the hippocampus, thalamus, and anterior insula. Absolute values of functional connectivity were reduced in regions included in the DM and dorsal attention regions compared to the resilient agers.

The 39 individuals in ABA subgroup 2 had more GM atrophy in the occipital, parietal, and orbitofrontal regions but not in the MTL or midbrain, in comparison to the reference group. They also showed greater functional coherence in the left temporal fusiform gyrus and greater connectivity bilaterally in the supramarginal gyrus.

ABA subgroup 3 comprised 62 individuals and showed focused bilateral atrophy in the hippocampus, thalamus, and superior temporal gyrus. Reduced coherence was found in the precuneus and left hippocampus. More importantly, group 3 showed significantly higher functional connectivity in the MTL SCP relative to the resilient group.

ABA subgroup 4 with 51 individuals showed GM atrophy in the entire midbrain, thalamus, and parieto-occipital medial regions, and somewhat of an orbitofrontal atrophy. Interestingly, this group showed significantly greater coherence bilaterally in the inferiomedial temporal cortex, temporal pole, and orbital-frontal regions. Connectivity was significantly lower between the bilateral opercular regions.

ABA subgroup 5 with 38 individuals showed the least pronounced differences from the resilient group. This group showed thalamus, precuneus, and hippocampal atrophies; reduced coherence in the posterior cerebellar regions; and reduced connectivity in the cerebellar, motor, and insular regions.

3.5. WMH in ABA subgroups

We compared total WMH volume between the resilient aging and 5 ABA subgroups, using 2-group t-tests. Advanced agers had a significantly higher WMH burden than resilient agers ($p < 10–4$). Of the 5 ABA subgroups, groups 1 and 5 had the highest WMH burden (significantly higher than the resilient group, $p < 10–5$). The WMH burden in ABA subgroup 3 was not significantly different from the resilient group ($p > 0.2$). Differences in WMH burden between the 5 ABA subgroups and the resilient aging group are summarized in Fig. 7. Pairwise group differences are reported in the Supplementary Information.

3.6. Cognitive performance in ABA subgroups

Figs. 8 and 9 plot estimates of the differences in cognition between each ABA subgroup and resilient group (labeled here as group 0) and their 95% confidence intervals. There were no significant differences in cognitive performance between resilient and the ABA subgroups combined. Pairwise comparisons of each ABA subgroup to the resilient group showed that the cognitive performance was both cross-sectionally and longitudinally worsening in ABA subgroup 1, compared to the resilient agers, on tests measuring verbal fluency and attention ($p < 0.05$). However, the difference was not significant for both tests after correction for multiple comparisons.

4. Discussion

Using advanced multivariate pattern analysis techniques, we revealed heterogeneity in the structural and functional variation associated with ABA, summarizing it by 5 main brain imaging phenotypes. The ABA subgroups showed notably distinct spatial patterns of structural and functional brain change in comparison to the reference group of resilient agers and differences in white matter lesion burden. Our results suggest that onset of pathology in older individuals is not a natural consequence of normal aging. Instead, a variety of underlying biological mechanisms are likely to be at play generating respective structural and functional imaging phenotypes.

To our knowledge, this is the first study to define the heterogeneity of ABA in a systematic and data-driven way using multivariate machine learning methods and capitalizing on a large cohort with 2 available modalities, structural and functional MRI. We would like to emphasize that ABA definition in our work is based on imaging patterns and not on cognitive status that demonstrate underlying factors leading to cognitively asymptomatic versus super agers (Harrison et al., 2012). A variety of genetic, demographic, and clinical factors may be associated with pathologic processes leading to functional and structural brain changes in older adults (Jagust, 2013), many years before cognitive impairment is evident (Jack et al., 2013). Separating “normal” from pathological aging in the preclinical phases of these disease states is a challenging task. Yet, it is of vital importance that we gain a better understanding of variations in ABA, so that we may identify distinct disease processes underlying this “accelerated” or “premature” brain changes. In addition to these subgroups potentially having different prognosis, they might also respond differentially to potential treatments, an issue of paramount importance in clinical trials. We believe that the heterogeneity of ABA patterns has been relatively unexplored to date, in part, because

commonly used approaches, such as the general linear models or even multivariate and machine learning analyses, seek single patterns of brain change, by construction.

Importantly, the ABA subgroups were not clustered along the direction of typical structural and functional brain aging values, as seen by their random distribution in Fig. 4. This suggests that these groups do not reflect different severity levels according to the derived aging indices but rather present heterogeneous patterns that were revealed by the full multivariate MOE analysis. Furthermore, the groups of advanced agers are not significantly different in terms of age or sex distribution, indicating that underlying pathologic mechanisms might develop in parallel and independently of age and sex in different individuals.

One of the striking findings of this study is that 3 of the 5 ABA subgroups (1, 3, and 4) demonstrate atrophy and altered functional integrity that involve regions and processes similar to those observed in neurodegenerative diseases, particularly AD. This is consistent with the observation that individuals in preclinical stages of disease may show greater structural and functional brain changes (Beason-Held et al., 2009; Pacheco et al., 2015). Continued follow-up of these individuals will help to further separate the age-related differences from those related to disease.

ABA subgroup 1 had the most pronounced pattern of brain change, with significant GM atrophy and reduced functional coherence and connectivity. Increased WMH in this group suggests presence of white matter—related vascular pathology. Results from cognitive data show that this group has also significantly greater longitudinal decline on measures of verbal fluency and attention in the years preceding and concurrent with the MRI scan. The relatively higher degeneration in the MTL, reduced coherence, and lower connectivity in regions included in the DM in subgroup 1 are generally consistent with findings in previous studies of aging and AD (Seeley et al., 2009; Sheline et al., 2010). Although global GM atrophy and reduced functional connectivity are observed in the absence of cognitive impairment, preferential reduction in midbrain structures, hippocampal GM density, and reduced DM connectivity is most pronounced in AD.

ABA subgroup 3 displayed imaging characteristics consistent with changes that have been associated with early AD pathology. We found focal hippocampal GM atrophy, reduced posterior cingulate/precuneus functional coherence, and relatively higher functional connectivity of the MTL, whereas the rest of the brain was not different from that of resilient agers. Similar patterns of greater connectivity have been previously reported in individuals with early stages of mild cognitive impairment (Bai et al., 2008; Dickerson et al., 2005; Sperling, 2011). It is possible that the functional hyperconnectivity of the study participants in this group could be a result of compensatory mechanisms for early neurodegeneration stages or even an early sign of hippocampal dysfunction (Sperling, 2011). Alternatively, high functional connectivity might reflect functional reserve in individuals who might otherwise have had declined cognitively. Interestingly, unlike the other ABA subgroups, this group had the lowest levels of comorbid WMH burden, which were similar to those in resilient agers. While recent studies demonstrated that the contribution of WMH to structural ABA (Habes et al., 2016a) and the relation of WMH to alterations in resting-state functional

connectivity in early AD (Zhou et al., 2015), our study extends upon such findings in showing the nonuniform presence of WMH throughout various ABA phenotypes.

ABA subgroup 4, compared with the resilient agers, showed significantly higher functional coherence in bilateral orbitofrontal and inferiomedial temporal regions, as well as increased coherence bilaterally in the inferiomedial temporal cortex and temporal pole. Greater coherence has been reported in studies investigating early stages of AD, in the right lingual gyrus and left fusiform gyrus (He et al., 2007).

Reduced function in motor and cerebellar regions was limited to individuals in ABA subgroup 5, which also showed signs of advanced midbrain and precuneus atrophies compared with resilient agers. Reduced brain function in these regions could possibly indicate impaired motor ability, which is prevalent among older people.

Our study has limitations. First, although the BLSA cohort is a longitudinal study, the rsfMRI scans were only available cross-sectionally, and we were unable to perform a longitudinal follow-up. Future studies will investigate the longitudinal trajectories of the phenotypic subtypes discovered herein. Second, the addition of amyloid and possibly tau imaging would be extremely useful for confirming the status of the cognitively normal individuals in ABA subgroups that show imaging patterns similar to those seen in AD. However, these imaging modalities were not available for this sample. Third, in the current analysis, we specifically investigated the heterogeneity in the ABA group, while the resilient to brain aging group was just used as a reference group. The current approach assumes that there is homogeneity within the reference group of healthy controls, which may not be the case, given the known variability in brain aging even in healthy people. We aim to explore this possible heterogeneity within the resilient to brain aging group in future studies. Fourth, an important limitation that should be acknowledged in the current report is the lack of validation of the ABA subgroups in an independent cohort. With validation in other cohorts, we hope that the use of these subtypes could facilitate selection of individuals for therapeutic interventions to delay onset or slow progression of neurodegenera- tive disease.

In conclusion, our results suggest that pathologic processes in older individuals could be reflected by heterogeneous imaging patterns of structural and functional brain changes with specific subtypes. A variety of underlying biological mechanisms are likely to be at play generating these phenotypes. The presented results enhance our understanding of the heterogeneity of brain aging and pave the way for developing translational diagnostic tools that can provide personalized indices of brain health.

Supplementary Material

Refer to Web version on PubMed Central for supplementary material.

Acknowledgements

This study was supported in part by NIH grant AG014971, the Intramural Research Program, National Institute on Aging, NIH, and NIA contract HHSN2712013000284P to the University of Pennsylvania. TDS was supported by NIMH R01MH10770. This work has been supported in part by NIH (grant no. 1RF1AG054409).

References

Bai F, Zhang Z, Yu H, Shi Y, Yuan Y, Zhu W, Zhang X, Qian Y, 2008 Default-mode network activity distinguishes amnestic type mild cognitive impairment from healthy aging: a combined structural and resting-state functional MRI study. Neurosci. Lett 438, 111–115. [PubMed: 18455308]

Beason-Held L, Kraut M, Resnick S, 2009 Stability of default-mode network activity in the aging brain. Brain Imaging Behav. 3, 123–131. [PubMed: 19568331]

Benjamini Y, Hochberg Y, 1995 Controlling the false discovery rate: a practical and powerful approach to multiple testing. J. R. Stat. Soc. Ser. B Methodol 57, 289–300.

Bezdek JC, 1981 Pattern Recognition With Fuzzy Objective Function Algorithms. Kluwer Academic Publishers, Springer, US, USA.

Boyle PA, Yang J, Yu L, Leurgans SE, Capuano AW, Schneider JA, Wilson RS, Bennett DA, 2017 Varied effects of age-related neuropathologies on the trajectory of late life cognitive decline. Brain J. Neurol 140, 804–812.

Brouwer RK, 2009 Extending the rand, adjusted rand and jaccard indices to fuzzy partitions. J. Intell. Inf. Syst 32, 213–235.

Cherubini A, Caligiuri ME, Peran P, Sabatini U, Cosentino C, Amato F, 2016 Importance of multimodal MRI in characterizing brain tissue and its potential application for individual age prediction. IEEE J. Biomed. Health Inform 20, 1232–1239. [PubMed: 27164612]

Ciric R, Wolf DH, Power JD, Roalf DR, Baum GL, Ruparel K, Shinohara RT, Elliott MA, Eickhoff SB, Davatzikos C, Gur RC, Gur RE, Bassett DS, Satterthwaite TD, 2017 Benchmarking of participant-level confound regression strategies for the control of motion artifact in studies of functional connectivity. Neuroimage 154, 174–187. [PubMed: 28302591]

Cole JH, Franke K, 2017 Predicting age using neuroimaging: innovative brain ageing biomarkers. Trends Neurosci. 40, 681–690. [PubMed: 29074032]

Dave RN, 1996 Validating fuzzy partitions obtained through c-shells clustering. Pattern Recognit. Lett 17, 613–623.

Dennis EL, Thompson PM, 2014 Functional brain connectivity using fMRI in aging and Alzheimer's disease. Neuropsychol. Rev 24, 49–62. [PubMed: 24562737]

Dickerson B, Salat D, Greve D, Chua E, Rand-Giovannetti E, Rentz D, Bertram L, Mullin K, Tanzi R, Blacker D, others, 2005 Increased hippocampal activation in mild cognitive impairment compared to normal aging and AD. Neurology 65, 404–411. [PubMed: 16087905]

Driscoll I, Resnick SM, Troncoso JC, An Y, O'Brien R, Zonderman AB, 2006 Impact of Alzheimer's pathology on cognitive trajectories in nondemented elderly. Ann. Neurol 60, 688–695. [PubMed: 17192929]

Eavani H, Hsieh MK, An Y, Erus G, Beason-Held L, Resnick S, Davatzikos C, 2016 Capturing heterogeneous group differences using mixture-of-experts: application to a study of aging. Neuroimage 125, 498–514. [PubMed: 26525656]

Eavani H, Satterthwaite TD, Filipovych R, Gur RE, Gur RC, Davatzikos C, 2015 Identifying Sparse Connectivity Patterns in the brain using resting-state fMRI. Neuroimage 105, 286–299. [PubMed: 25284301]

Franke K, Ziegler G, Klöppel S, Gaser C, 2010 Estimating the age of healthy subjects from T1-weighted {MRI} scans using kernel methods: exploring the influence of various parameters. Neuroimage 50, 883–892. [PubMed: 20070949]

Gaser C, Franke K, Klöppel S, Koutsouleris N, Sauer H, Initiative ADN, 2013 BrainAGE in mild cognitive impaired patients: predicting the conversion to Alzheimer's disease. PLoS One 8, e67346. [PubMed: 23826273]

Habes M, Erus G, Toledo JB, Zhang T, Bryan N, Laune LJ, Rosseel Y, Janowitz D, Doshi J, Van der Auwera S, von Sarnowski B, Hegenscheid K, Hosten N, Homuth G, Völzke H, Schminke U, Hoffmann W, Grabe H, Davatzikos C, 2016a White matter hyperintensities and imaging patterns of brain aging in the general population. Brain 139 (Pt 4), 1164–1179. [PubMed: 26912649]

Habes M, Janowitz D, Erus G, Toledo J, Resnick SM, Doshi J, Auwera SV, der Wittfeld K, Hegenscheid K, Hosten N, Biffar R, Homuth G, Völzke H, Grabe HJ, Hoffmann W, Davatzikos C,

2016b Advanced Brain Aging: relationship with epidemiologic and genetic risk factors, and overlap with Alzheimer disease atrophy patterns. Transl Psychiatry 6, e775. [PubMed: 27045845]

Harrison TM, Weintraub S, Mesulam M-M, Rogalski E, 2012 Superior memory and higher cortical volumes in unusually successful cognitive aging. J. Int. Neuropsychol. Soc. JINS 18,1081–1085. [PubMed: 23158231]

He Y, Wang L, Zang Y, Tian L, Zhang X, Li K, Jiang T, 2007 Regional coherence changes in the early stages of Alzheimer's disease: a combined structural and resting-state functional MRI study. Neuroimage 35, 488–500. [PubMed: 17254803]

Honnorat N, Eavani H, Satterthwaite T, Gur RE, Gur RC, Davatzikos C, 2015 GraSP: geodesic graph-based segmentation with Shape priors for the functional parcellation of the cortex. Neuroimage 106, 207–221. [PubMed: 25462796]

Jack CR, Knopman DS, Jagust WJ, Petersen RC, Weiner MW, Aisen PS, Shaw LM, Vemuri P, Wiste HJ, Weigand SD, Lesnick TG, Pankratz VS, Donohue MC, Trojanowski JQ, 2013 Tracking pathophysiological processes in Alzheimer's disease: an updated hypothetical model of dynamic biomarkers. Lancet Neurol. 12, 207–216. [PubMed: 23332364]

Jagust W, 2013 Vulnerable neural systems and the borderland of brain aging and neurodegeneration. Neuron 77, 219–234. [PubMed: 23352159]

Lao Z, Shen D, Liu D, Jawad AF, Melhem ER, Launer LJ, Bryan RN, Davatzikos C, 2008 Computer-assisted segmentation of white matter lesions in 3D {MR} images using Support vector machine. Acad. Radiol 15, 300–313. [PubMed: 18280928]

Liem F, Varoquaux G, Kynast J, Beyer F, Kharabian Masouleh S, Huntenburg JM, Lampe L, Rahim M, Abraham A, Craddock RC, Riedel-Heller S, Luck T, Loeffler M, Schroeter ML, Witte AV, Villringer A, Margulies DS, 2017 Predicting brain-age from multimodal imaging data captures cognitive impairment. Neuroimage 148, 179–188. [PubMed: 27890805]

Pacheco J, Goh JO, Kraut MA, Ferrucci L, Resnick SM, 2015 Greater cortical thinning in normal older adults predicts later cognitive impairment. Neurobiol. Aging 36, 903–908. [PubMed: 25311277]

Pievani M, de Haan W, Wu T, Seeley WW, Frisoni GB, 2011 Functional network disruption in the degenerative dementias. Lancet Neurol. 10, 829–843. [PubMed: 21778116]

Prins ND, Scheltens P, 2015 White matter hyperintensities, cognitive impairment and dementia: an update. Nat. Rev. Neurol 11, 157–165. [PubMed: 25686760]

Rachael IS, Frost C, Jenkins R, Whitwell JL, Rossor MN, Fox NC, 2003 A longitudinal study of brain volume changes in normal aging using serial registered magnetic resonance imaging. Arch. Neurol 60, 989–994. [PubMed: 12873856]

Raz N, Lindenberger U, Rodrigue KM, Kennedy KM, Head D, Williamson A, Dahle C, Gerstorf D, Acker JD, 2005 Regional brain changes in aging healthy adults: general trends, individual differences and modifiers. Cereb. Cortex 15, 1676–1689. [PubMed: 15703252]

Resnick SM, Pham DL, Kraut MA, Zonderman AB, Davatzikos C, 2003 Longitudinal magnetic resonance imaging studies of older adults: a shrinking brain. J. Neurosci 23, 3295–330. [PubMed: 12716936]

Satterthwaite TD, Elliott MA, Gerraty RT, Ruparel K, Loughead J, Calkins ME, Eickhoff SB, Hakonarson H, Gur RC, Gur RE, others, 2013 An improved framework for confound regression and filtering for control ofmotion artifact in the preprocessing of resting-state functional connectivity data. Neuroimage 64, 240–256. [PubMed: 22926292]

Seeley WW, Crawford RK, Zhou J, Miller BL, Greicius MD, 2009 Neurodegenerative diseases target large-scale human brain networks. Neuron 62, 42–52. [PubMed: 19376066]

Sheline YI, Raichle ME, 2013 Resting state functional connectivity in preclinical Alzheimer's disease. Biol. Psychiatry 74, 340–34. [PubMed: 23290495]

Sheline YI, Raichle ME, Snyder AZ, Morris JC, Head D, Wang S, Mintun MA, 2010 Amyloid plaques disrupt resting state default mode network connectivity in cognitively normal elderly. Biol. Psychiatry 67, 584–587. [PubMed: 19833321]

Sperling R, 2011 The potential of functional MRI as a biomarker in early Alzheimer's disease. Neurobiol. Aging 32, S37–S43. [PubMed: 22078171]

Whitwell JL, Petersen RC, Negash S, Weigand SD, Kantarci K, Ivnik RJ, Knopman DS, Boeve BF, Smith GE, Jack CR, 2007 Patterns of atrophy differ among specific subtypes of mild cognitive impairment. Arch. Neurol 64, 1130–1138. [PubMed: 17698703]

Zang Y, Jiang T, Lu Y, He Y, Tian L, 2004 Regional homogeneity approach to fMRI data analysis. Neuroimage 22, 394–400. [PubMed: 15110032]

Zhou Y, Yu F, Duong TQ, 2015 White matter lesion loadis associated with resting state functional MRI activity and amyloid PET but not FDG in mild cognitive impairment and early Alzheimer's disease patients. J. Magn. Reson. Imaging JMRI 41, 102–109. [PubMed: 24382798]

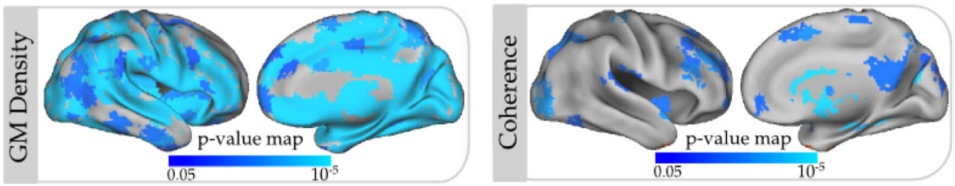

Fig. 1.

Aging-related changes in GM density and functional coherence. Significance maps show significant voxelwise correlations between imaging measures and age, with $p < 0.05$, corrected for multiple comparisons. The significance maps are shown in blue-light blue color map, projected on the brain cortical surface. In the highlighted areas, GM density and functional coherence values show a significant decrease with age. Abbreviation: GM, gray matter. (For interpretation of the references to color in this figure legend, the reader is referred to the Web version of this article.)

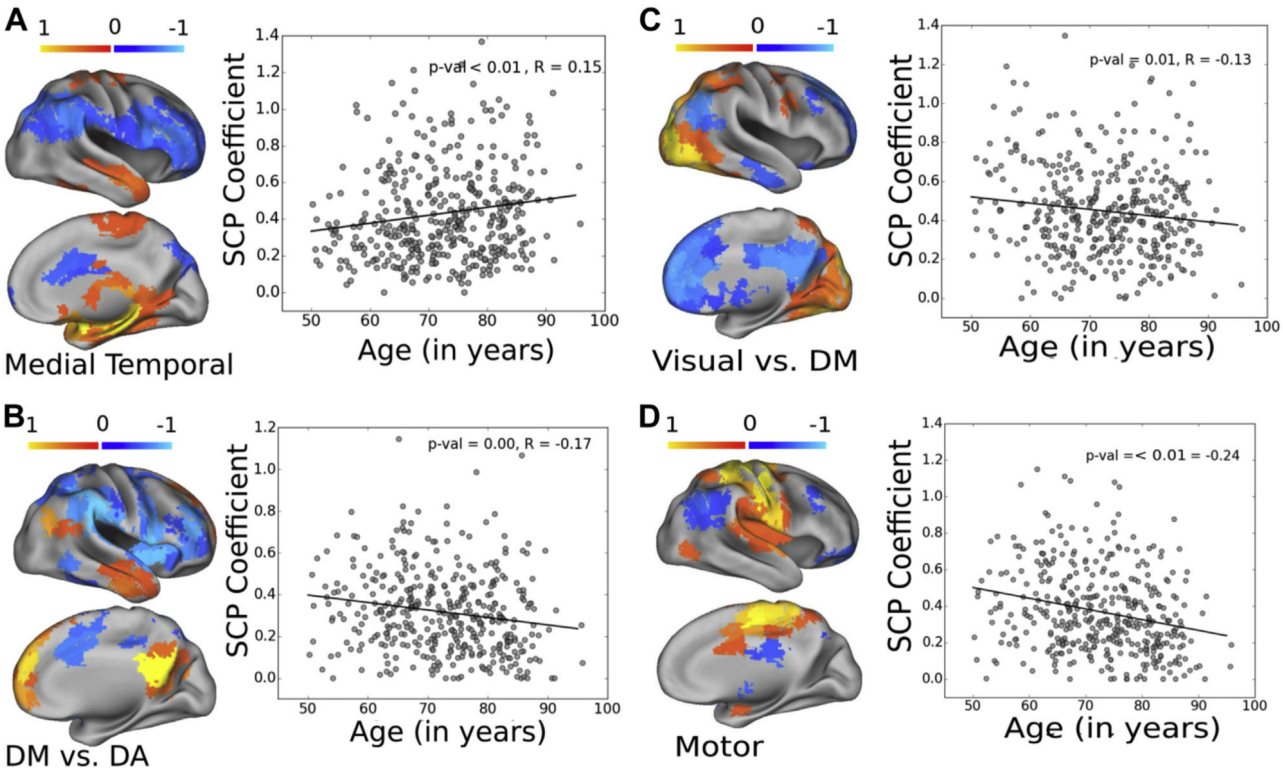

Fig. 2.

Aging effects in SCP coefficients. From the 10 SCPs, 4 have shown significant correlations with age ($p < 0.05$, corrected for multiple corrections). Connectivity within the SCP that delineates medial temporal areas was significantly higher with age (R = 0.15, panel A); connectivity within the default mode versus dorsal attention SCP (R = −0.17, panel B), within the visual versus default mode areas (R = −0.13, panel C) and within the motor areas (panel D) were significantly lower with age (R = −0.24, panel D). Abbreviations: DA, dorsal attention; DM, default mode; SCP, sparse connectivity pattern.

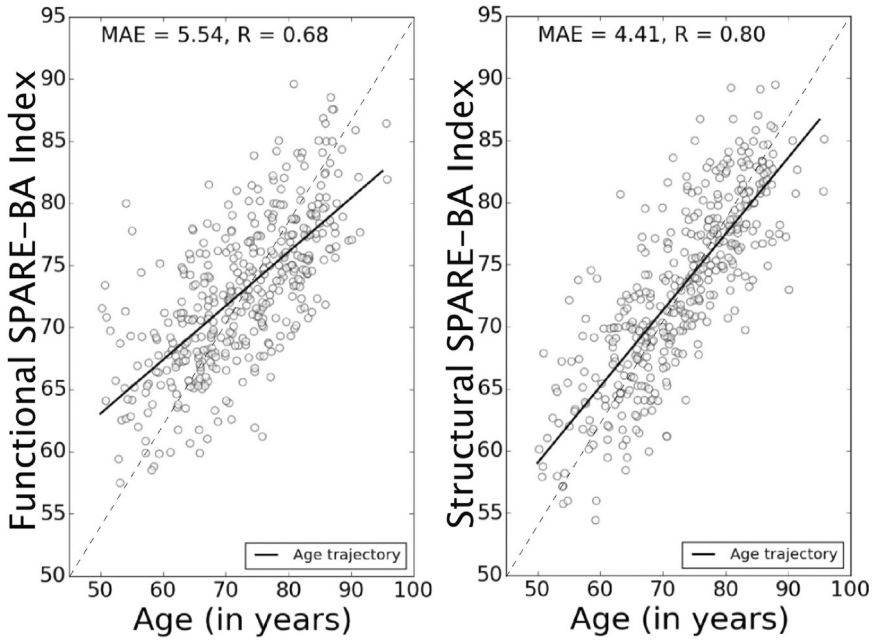

Fig. 3.

Structural and functional SPARE-BA values of BLSA participants against their actual age. SPARE-BA values were calculated using cross-validation. Abbreviations: BLSA, Baltimore Longitudinal Study of Aging; MAE, mean average error; SPARE-BA, Spatial Patterns of Brain Alteration for capturing brain aging.

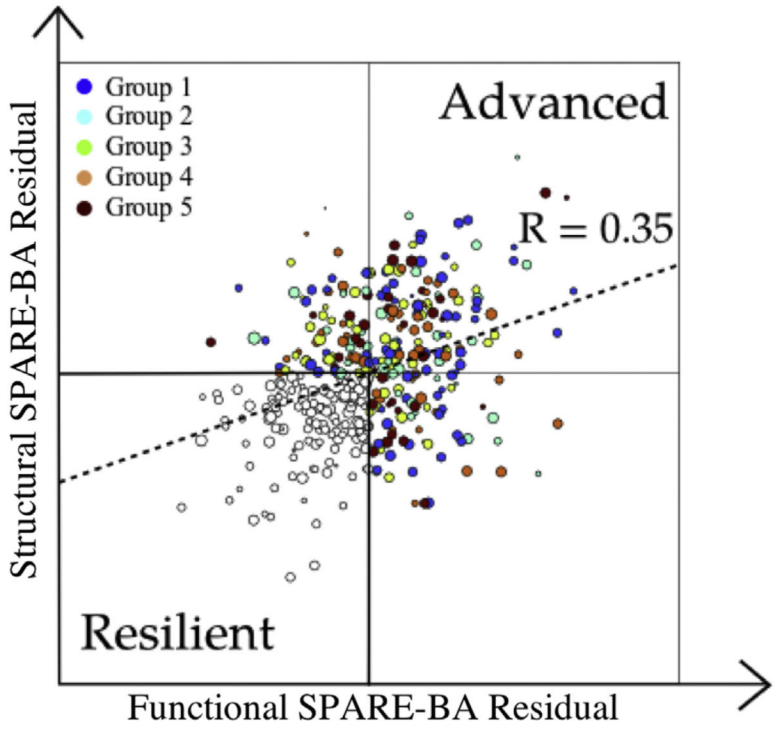

Fig. 4.

The residuals of structural and functional SPARE-BA indices plotted on a 2-dimensional grid. A higher value of the residual for each index indicates that an individual's brain age is higher than the expected typical brain age, and vice versa. Accordingly, study participants are categorized as resilient agers (both structural and functional residuals are negative) or as advanced brain agers (ABA, at least one of the residuals is positive). The size of each circle is proportional to the age of the individual. The color codes show the ABA subcategory of each ABA individual, which was automatically determined using a semisupervised algorithm. Abbreviations: ABA, advanced brain aging; SPARE-BA, Spatial Patterns of Brain Alteration for capturing brain aging. (For interpretation of the references to color in this figure legend, the reader is referred to the Web version of this article.)

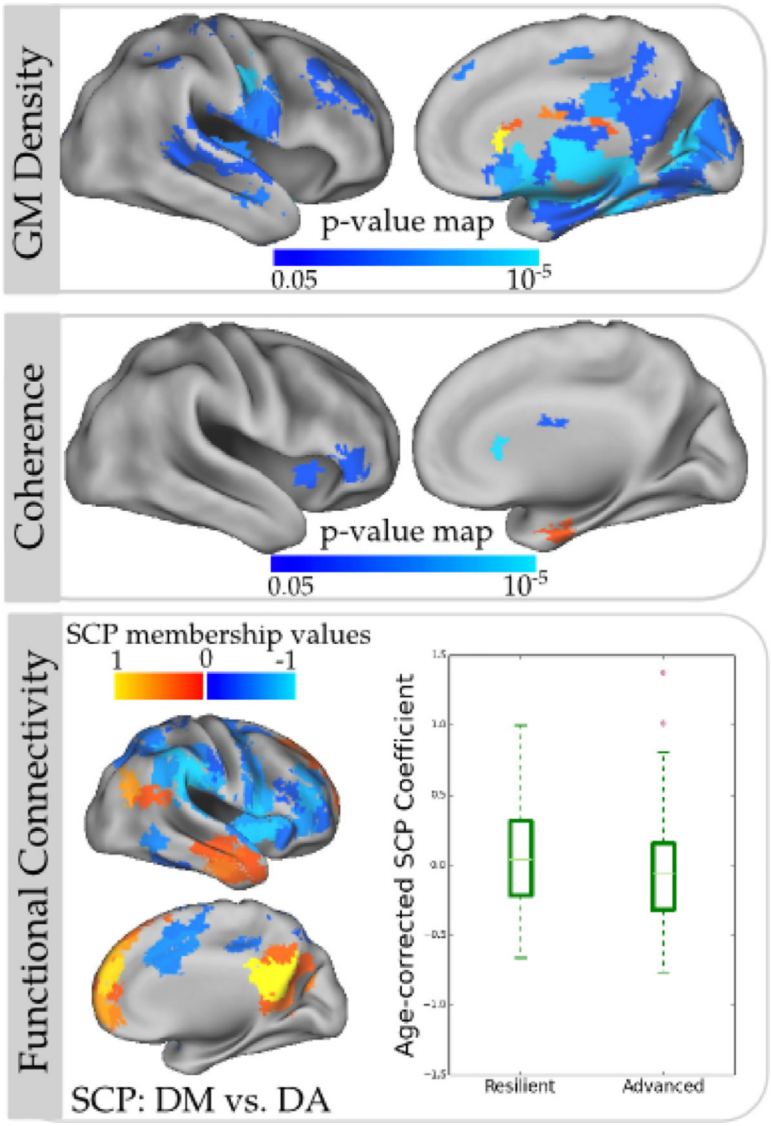

Fig. 5.

Group differences between individuals in resilient and ABA groups in GM density (top), functional coherence (middle), and functional connectivity (bottom). The significance maps for GM density and functional coherence are shown in blue-light blue color map, projected on the brain cortical surface. In the highlighted areas, GM density and functional coherence values for ABA study participants are significantly lower ($p < 0.05$, corrected for multiple comparisons). From the 10 SCPs, only 1, the SCP that groups the default mode versus dorsal attention, has shown significant group differences between the 2 groups ($p < 0.05$, corrected for multiple corrections). The overlay indicates a spatial pattern of correlated regions; opposing colors (red-yellow vs. blue-light blue) reflect anticorrelated regions. The mean and standard error of the associated SCP coefficient for both groups are plotted to the right. Note that the color overlay for the SCP indicates patterns of correlated (or anticorrelated) regions and is not related to statistical significance. Abbreviations: ABA, advanced brain aging; GM,

gray matter; SCP, sparse connectivity pattern. (For interpretation of the references to color in this figure legend, the reader is referred to the Web version of this article.)

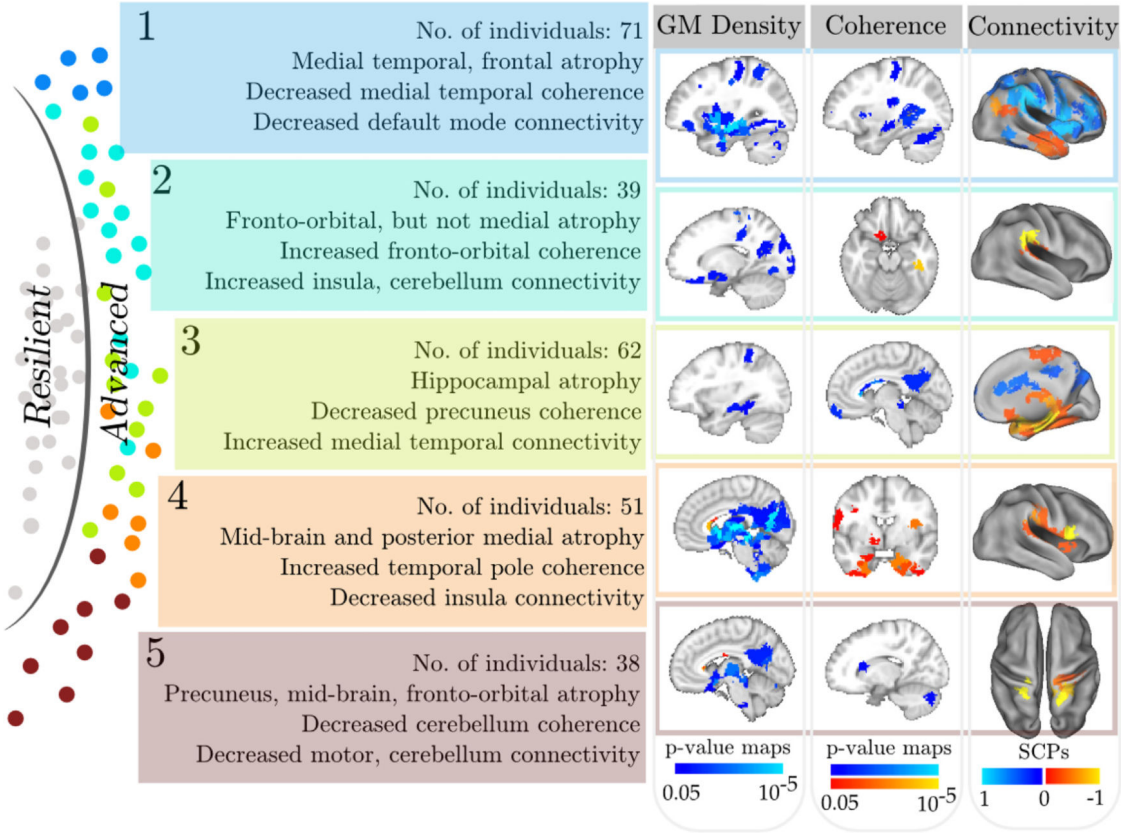

Fig. 6.

Group differences between individuals in resilient and 5 automatically detected ABA subgroups in GM density, functional coherence, and connectivity. Similar to Fig. 5, changes to GM density and functional coherence at the level of ROIs are shown using p-value maps overlaid on a template image (first 2 columns on the right). For the coherence data (middle column), the positive color scale (red-yellow) reflects increased coherence (direction of change), although both color scales are equivalent in terms of p-values. SCPs whose connectivity was significantly altered are shown in the last column. Note that the color overlay for SCPs indicates patterns of correlated (or anticorrelated) regions and is not related to statistical significance. Abbreviations: ABA, advanced brain aging; GM, gray matter; ROI, regions of interest; SCP, sparse connectivity pattern. (For interpretation of the references to color in this figure legend, the reader is referred to the Web version of this article.)

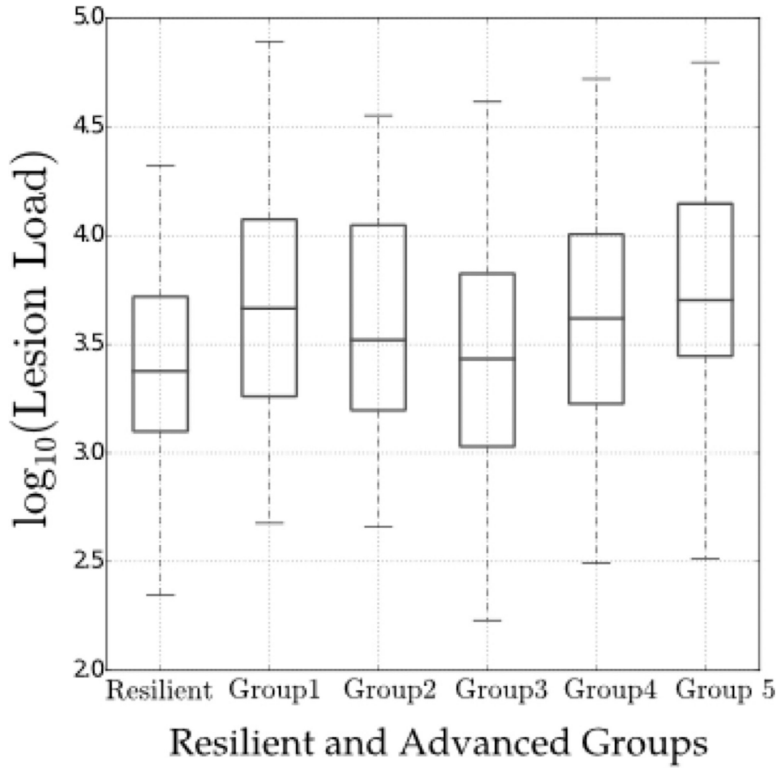

Fig. 7.

Total WMH burden of individuals in the resilient aging group and in each of the 5 ABA subgroups. The values are converted to log scale due to skewed distribution of them. The box plots indicate mean values and standard deviation. Abbreviations: ABA, advanced brain aging; WMH, white matter hyperintensities.

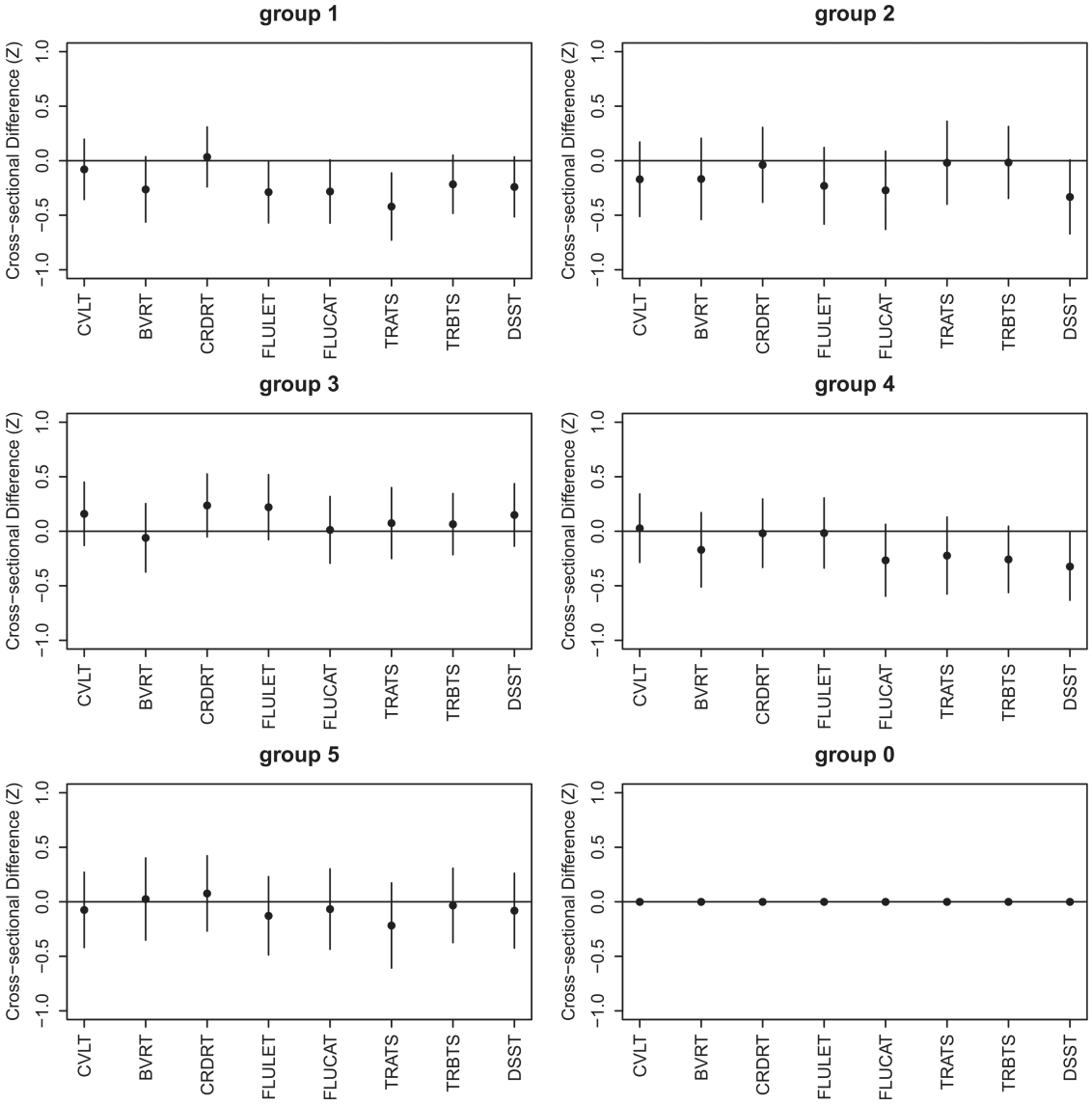

Fig. 8.

Cross-sectional cognitive performance of individuals in each of the 5 ABA subgroups, in comparison to the resilient group (denoted as group 0). Ninety-five percentage confidence intervals are shown as error bars. Abbreviations: ABA, advanced brain aging; BVRT, Benton Visual Retention Test; CRDRT, Card Rotations Test; CVLT, California Verbal Learning Test; DSST, Digit Span subtest from the Wechsler Adult Intelligence Scale—Revised; FLUCAT, Verbal fluency categories; FLULET, Verbal fluency letters; TRATS, Trail Making Test parts Total Score A; TRBTS, Trail Making Test parts Total Score B; WMH, white matter hyperintensity.

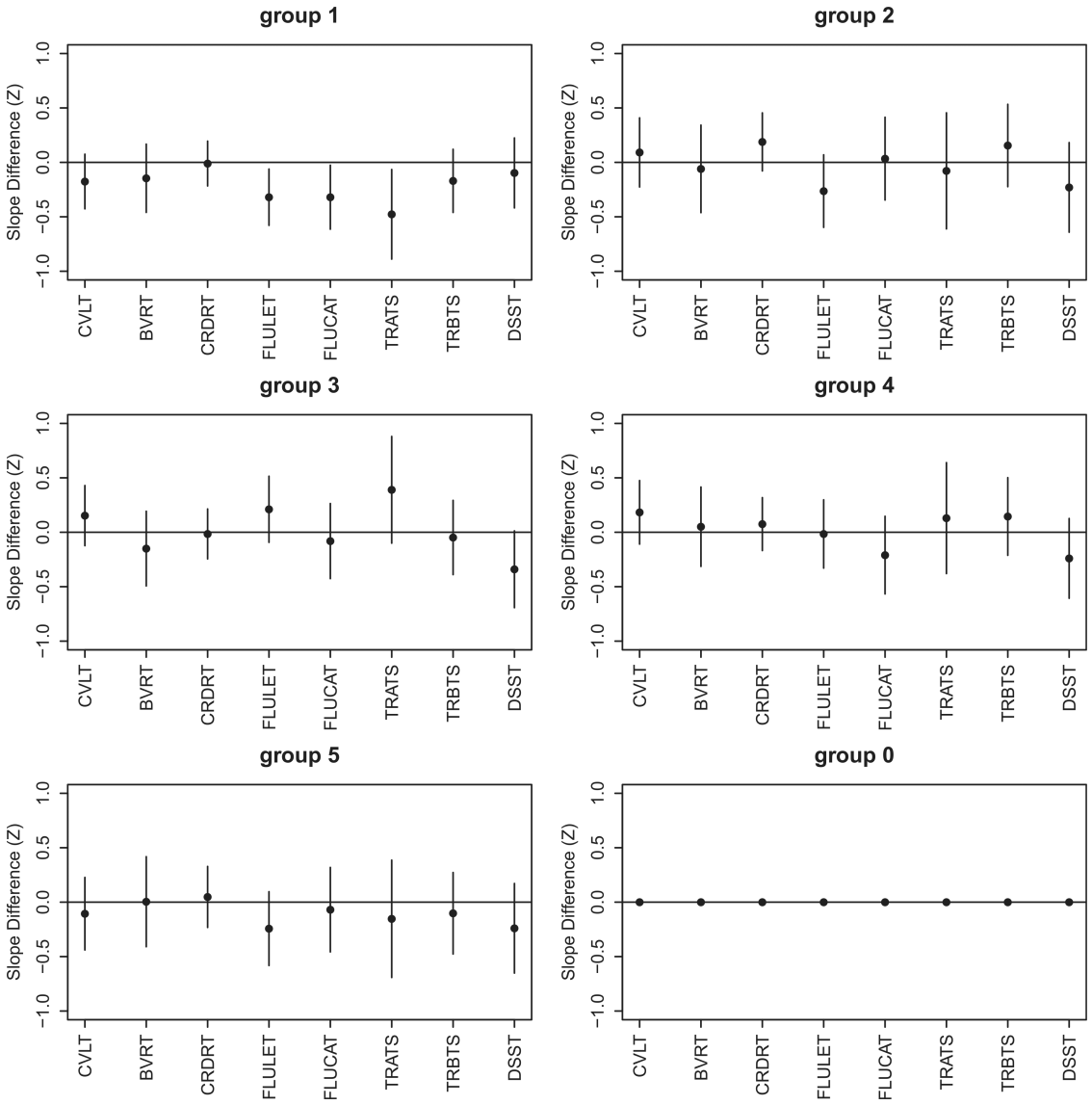

Fig. 9.

Rate of change of cognitive performance of individuals in each of the 5 ABA subgroups, in comparison to the resilient group (denoted as group 0). Ninety-five percentage confidence intervals are shown as error bars. Abbreviation: ABA, advanced brain aging; BVRT, Benton Visual Retention Test; CRDRT, Card Rotations Test; CVLT, California Verbal Learning Test; DSST, Digit Span subtest from the Wechsler Adult Intelligence Scale—Revised; FLUCAT, Verbal fluency categories; FLULET, Verbal fluency letters; TRATS, Trail Making Test parts Total Score A; TRBTS, Trail Making Test parts Total Score B.

Table 1

Demographics and motion variables associated with resilient and advanced aging groups

	Resilient	Advanced 1	Advanced 2	Advanced 3	Advanced 4	Advanced 5
N	139	71	39	62	51	38
Age	72.2 ± 8.8	73.5 ± 9.1	72.9 ± 10.8	72.75 ± 9.4	70.0 ± 10.0	72.8 ± 10.5
Sex (male)	57	37	23	36	7	9
Frames scrubbed	4.0 ± 6.5	7.5 ± 7.6	6.8 ± 7.4	6.5 ± 8.1	3.7 ± 5.9	5.0 ± 7.7